ASCE Journal of Offshore Mechanics and Arctic Engineering
In Press for May 2010, Volume 132, Issue 2
Slightly revised here to clarify kappa and include Eqs 8--10

The Hermite Moment Model for Highly Skewed Response with Application to Tension Leg Platforms

Myoungkeun Choi* and Bert Sweetman†

Department of Civil Engineering, Texas A&M University

3136 TAMU, College Station, TX 77843-3136, USA

A new addition to the statistical Hermite moment model of extremes is introduced for use on processes with high skewness and near-Gaussian kurtosis. The monotone limits of the existing model are expressed as ellipses in response moment space and a new methodology is introduced that combines hardening and softening models to overcome these limits. The result is that any fractile of a distribution described by its first four statistical moments can be transformed to or from the Gaussian. An example application to a Tension Leg Platform is presented.

1 INTRODUCTION

Many irregular time-series processes exhibit non-Gaussian behavior. In some specific cases, response of systems subject to irregular excitation have been shown to be well represented by a Gaussian random process. However, other structural systems often have response processes with meaningfully larger or smaller extreme values than would be predicted directly from Gaussian theory. This non-Gaussian behavior may result from nonlinear structural response characteris-

*Myoungkeun Choi: E-mail: myoungchoi@gmail.com, Telephone: (281) 870-5604, Fax:(281) 870-5210

†Bert Sweetman: E-mail: sweetman@tamu.edu, Telephone:(409) 740-4834, Fax:(409) 741-7153

tics, nonlinear excitation loads, or both. For such systems, direct use of Gaussian statistics is not appropriate.

Theoretically simple methods, such as direct Monte Carlo simulation of very large data-sets, are increasingly relevant as computational power continues to become more readily available. This methodology includes use of numerical time stepping direct integration methods to simulate a large number of time-series, the results of which are subsequently used to develop a full probability distribution for use in prediction of upcrossing rates, extreme values, and fatigue damage. Unfortunately, these methods are limited to physical processes for which time-series can be accurately simulated, including the extreme events. In some cases meaningful simulation is not possible, so extreme events must be predicted based on data which as been measured. In these cases, sufficient data to construct full probability distributions are rarely available. Similarly, in cases where the statistical moments of a probability distribution are already known, computer simulation of the process to predict specific fractiles of the response is difficult and inelegant at best. Application to this latter class of problems is what motivated the authors to develop this extension to the Hermite methodology.

Other, less computationally intensive, alternatives to direct simulation methods are also available, including various approximation approaches such as equivalent linearization techniques and series distribution methods. Equivalent linearization techniques [1, 3, 18] are only useful to estimate gross response statistics such as root mean square levels. Series distribution methods [6, 13] can be used to transform known statistical results such as mean upcrossing rates and extreme values of a Gaussian process into those of a non-Gaussian process by finding a simple functional transformation of the equivalent Gaussian statistics.

Full probability distributions of a non-Gaussian process can be estimated using Gram-Charlier series, Edgeworth series, and Longuet-Higgins series from those of a Gaussian process e.g. [12, 13, 17]. These series distribution methods have a common weakness: they all tend to exhibit oscillating and negative tail behavior. Overcoming this weakness, the Hermite moment model was

developed and shown to be more flexible over a wider range of skewness and kurtosis values [19, 20]. This Hermite moment model offers equivalent fractile mapping between Gaussian and non-Gaussian processes and has been widely applied to a variety of areas: non-Gaussian excitation and structural response estimation e.g. [7], extreme response estimation e.g. [14], non-Gaussian wave kinematics estimation e.g. [11], and non-Gaussian simulation e.g. [15]. There are, however, some processes to which the transformation is not directly applicable. Non-monotone transformations complicate application to processes with high skewness but near-Gaussian kurtosis. This paper begins with a review of the theory underlying the Hermite moment model, with special emphasis on this monotone limit.

2 BACKGROUND: THE FOUR-MOMENT HERMITE MODEL

The four-moment Hermite model uses skewness and kurtosis to transform between standardized Gaussian and equivalent non-Gaussian fractiles. This paper addresses both forward and backward transformations: the forward transformation maps fractiles of a Gaussian process to those of a non-Gaussian, and the backward transformation maps fractiles of a non-Gaussian process to Gaussian equivalents. Additionally, any non-Gaussian process can be softening, hardening, or a combination of the two. The probability distribution of a softening process has thicker tails than a Gaussian distribution. An example softening process would be the irregular dynamic response of a spring-mass system to a Gaussian excitation if the spring is non-linear, with stiffness that decreases with increasing displacement (softens). Such a system would have relatively greater maxima and smaller minima than would an equivalent system with a linear spring. Conversely, the probability distribution of a hardening process has thinner tails than the Gaussian distribution.

The four-moment Hermite model for transformation of a process that is relatively thin-tailed to a process that is thicker-tailed over the entire fractile range is a cubic polynomial. The polynomial applies to either forward transformation of a softening process (from Gaussian to non-Gaussian) or backward transformation of a hardening process (from non-Gaussian to Gaussian). Transforma-

tions from processes with relatively thick-tailed distributions to thinner-tailed distributions require inversion of the cubic polynomial. The model developed by Winterstein [19, 20] has two limitations: 1) the monotone limit, which enables a simple inversion of the cubic polynomial over the entire fractile range, and 2) a practical limit predicted by the underlying theory defining theoretically impossible combinations of skewness and kurtosis values. This paper provides an alternative inversion methodology that is not subject to the monotone limit.

2.1 The Functional Form of the Transformation

The Hermite moment model transforms any fractile between standardized Gaussian and non-Gaussian processes, such that the cumulative distribution function (CDF) of a standard non-Gaussian process matches that of the standard Gaussian. The model for mapping a relatively thin-tailed process to a thicker-tailed process has a simple form resulting from an infinite series polynomial expansion. The first few terms of the expansion can be conveniently and appropriately applied to transform between specific fractiles.

$$x = a_0 + a_1 P_1(u) + a_2 P_2(u) + a_3 P_3(u) + ... \quad (1)$$

$$u = b_0 + b_1 P_1(x) + b_2 P_2(x) + b_3 P_3(x) + ... \quad (2)$$

where x and u are values of random variables X and U, and $P_j(\cdot)$ indicates the $j'th$ term of a polynomial expansion that possesses orthogonal properties. Standardized random variables are used throughout this paper: $X = \frac{Y-\mu_Y}{\sigma_Y}$ and $U = \frac{V-\mu_V}{\sigma_V}$ represent standard non-Gaussian and standard Gaussian processes, respectively; argument t is omitted for brevity. μ_Y, σ_Y, α_3 and α_4 are the mean, standard deviation, skewness and kurtosis of a non-Gaussian process Y. μ_V and σ_V are the mean and standard deviation of a Gaussian process V.

Winterstein [19, 20] provides an infinite-series polynomial expansion and a representation of the functional transformation with four terms, whose coefficients are directly related to the response moments of the non-Gaussian process. A non-Gaussian softening process can be expressed

by a Hermite polynomial series expansion of the Gaussian process:

$$x = \kappa\Big\{u + \sum_{n=3}^{N=\infty} h_n \mathrm{He}_{n-1}(u)\Big\} \tag{3}$$

$$\simeq \kappa\Big\{u + h_3(u^2-1\Big) + h_4\Big(u^3 - 3u)\Big\} \tag{4}$$

where κ is a scale factor that ensures x has unit variance. He_n is the n^{th} Hermite polynomial: $\mathrm{He}_1(\xi) = \xi$, $\mathrm{He}_2(\xi) = \xi^2 - 1$, $\mathrm{He}_3(\xi) = \xi^3 - 3\xi$, etc., where ξ is any value. Coefficients h_3 and h_4 are directly calculated from the skewness and kurtosis of the non-Gaussian process. Similarly, a Gaussian response can be expressed by a Hermite polynomial series expansion of a hardening response process:

$$u = x - \sum_{n=3}^{\infty} h_n \mathrm{He}_{n-1}(x) \tag{5}$$

$$\simeq x - h_3(x^2-1) - h_4(x^3 - 3x) \tag{6}$$

In both transformations, the Hermite polynomial coefficients h_n give shape to the resulting distributions. Taking only first-order terms of the expansion yields direct relationships between the first n Hermite coefficients and the first n statistical moments of the standardized non-Gaussian variable [19, 20].

$$h_1 = h_2 = 0, \qquad h_3 = \frac{\alpha_3}{6}, \qquad h_4 = \frac{\alpha_4 - 3}{24} \tag{7}$$

Truncating the infinite expansion at the first four response moments makes the implicit assumption that terms higher than h_4 are negligible. In practice, use of response moments higher than the kurtosis is difficult because of high variability in sampling these higher moments. If the nonlinearity is sufficiently mild that terms of the order $h_n h_m$ can be neglected, it can be shown that $\kappa = 1$. In addition to these first-order coefficients, Winterstein developed second-order coefficients for the forward softening case by taking all the first- and second-order terms in the expansion and including terms of the order $h_n h_m$ [19, 20]:

$$h_3 = \frac{\alpha_3}{4 + 2\sqrt{1 + 1.5(\alpha_4 - 3)}} \tag{8}$$

$$h_4 = \frac{\sqrt{1 + 1.5(\alpha_4 - 3)} - 1}{18} \tag{9}$$

$$\kappa = (1 + 2h_3^2 + 6h_4^2)^{-1/2} \tag{10}$$

Other second-order representations are proposed in [10, 22]. In later work, Winterstein and Lange [9, 21] proposed computational methods to find optimized coefficients by minimizing the sum of squared errors.

2.2 Inversion

Equations 4 and 6 directly map thin- to thick-tailed distributions; mapping from thick- to thin-tailed distributions requires inversion of the polynomial transformation. Winterstein does not provide an inversion of Equation 6; he does provide an inversion of Equation 4, which is applicable only inside the monotone limits (Section 3):

$$u = \left[\sqrt{\xi^2(x) + c} + \xi(x)\right]^{1/3} - \left[\sqrt{\xi^2(x) + c} - \xi(x)\right]^{1/3} - a \tag{11}$$

$$\text{where} \qquad \xi(x) = 1.5b\left(a + \frac{x}{\kappa}\right) - a^3$$

$$a = \frac{h_3}{3h_4}, \qquad b = \frac{1}{3h_4}, \qquad c = \left(b - 1 - a^2\right)^3$$

In addition to the monotone limit, a square root in Equation 11 requires that $\xi^2(x) + c$ be non-negative.

Figure 1 shows the various regions where each of the transformation pairs is applicable. The curved lines are the monotone and practical limits, which divide the space into various regions. In regions I and II the original polynomials are applicable (Equations 4 and 6). The pre-existing inversion is only applicable in region I (Equation 11). Here, a new inversion is offered for use in region II as is a new methodology for use in regions III and IV. The new method is applicable to either forward or backward transformations. Skewness and kurtosis combinations outside the practical limit are extremely rare, and use of the Hermite model would generally not be useful or justified (I_X, II_X, III_X, and IV_X).

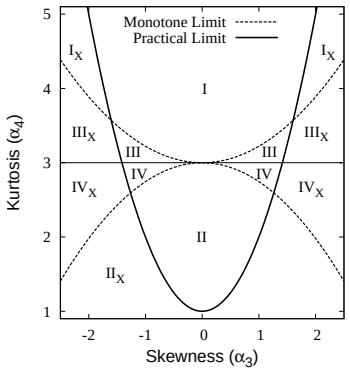

Figure 1: Various Regions of Model Applicability

2.3 Limitations of the Original Hermite Model of Extremes

The parabolic curve shown with a solid line on Figure 1 represents a practical limit based on a polynomial expansion.

$$\alpha_4 \geq \alpha_3^2 + 1 \tag{12}$$

The infinite-series expansion on which this transformation model is based predicts skewness-kurtosis combinations will not occur in regions below this parabola. It is in fact possible to create highly skewed distributions in violation of this limit, and the Hermite transformations are generally smooth and well-behaved as they cross the limit. However, these cases are so far beyond the reasonable limits of second-order theory that use of the model is not appropriate. The original development by Winterstein [19] includes a cogent explanation; some of his most salient points are closely paraphrased here:

> Various results of any random process $Z(t)$ can be expressed as a sum of n polynomials, $P_n[Z(t)]$, that possess orthogonal properties:
>
> $$E[P_n(Z)] = E[P_n(Z)P_m(Z)] = 0 \qquad (n \neq m; \quad n, m > 0) \tag{13}$$
>
> The n^{th} such polynomial can be constructed from the simple power law $Z^n(t)$ by

removing its correlation with all lower order polynomials:

$$P_n(Z) = Z^n - \sum_{k=0}^{n-1} c_{nk} P_k(Z); \qquad c_{nk} = \frac{E[Z^n P_k(Z)]}{E[P_k^2(Z)]} \tag{14}$$

If $Z(t)$ has been standardized to have zero mean and unit variance, applying Equation 14 with $P_0(Z) = 1$ leads to the polynomials

$$P_1(Z) = Z; \qquad P_2(Z) = Z^2 - \alpha_3 Z - 1; \tag{15}$$

$$P_3(Z) = Z^3 - c_{32} P_2(Z) - \alpha_4 Z - \alpha_3; \qquad \ldots \tag{16}$$

in which $c_{32} = E[Z^3 P_2(Z)]/E[P_2^2(Z)] = (\alpha_5 - \alpha_3 - \alpha_3\alpha_4)/(\alpha_4 - \alpha_3^2 - 1)$. Noting that the $E[P_2^2(Z)] = \alpha_4 - \alpha_3^2 - 1$ cannot be negative, the kurtosis value, α_4 cannot be less than $\alpha_3^2 + 1$.

That final observation, $\alpha_4 \geq \alpha_3^2 + 1$, constitutes the practical limit.

Winterstein goes on to show that various generalizations of this model can be formed from these orthogonal polynomials, including the ability to model a new random process from only its first N moments; one such example is the Hermite model of extremes. As the distribution of a non-Gaussian process approaches a Gaussian through the infinite-series approximation, the orthogonality condition of Equation 13 is used to ensure several important properties. Most importantly, 1) it ensures that the polynomial moments are the central moments of the process and 2) that polynomials of order higher than N are equal to zero or at least negligible. The orthogonality of the polynomials also guarantees uniqueness of the Hermite coefficients. In the next section, the monotone limits are fully explained and represented geometrically as ellipses in moment space. Alternate solutions are then offered that yield results identical to those of Winterstein in the monotone regions, and also enable application of the model over the entire range within the practical limit, i.e., the entire range for which the model is likely to be useful.

3 OVERCOMING THE MONOTONE LIMITATION

One of the principal contributions of this paper is an alternative implementation of the Hermite polynomial that overcomes the monotone limitation. First, the monotone limits are investigated numerically and represented geometrically, then the results are used to develop a new inversion and a new alternative methodology to construct monotonic transformations for non-monotone regions.

3.1 Understanding the Monotone Limits

Figure 2 is developed later in this section. The horizontal and vertical axes are the coefficients of the Hermite polynomials: $h_3 = \alpha_3/6$, and $h_4 = (\alpha_4 - 3)/24$. The Hermite polynomial transformation is shown to be monotone inside each ellipse and non-monotone outside. The regions in Figure 1 depict the five possible cases:

I. The two coefficients, h_3 and h_4, are inside the upper ellipse ($D_s \leq 0$), which indicates the transformation for softening response increases monotonically.

II. The two coefficients are inside the lower ellipse ($D_h \leq 0$), which indicates the transformation for hardening response increases monotonically.

III. The two coefficients are outside the upper ellipse as well as above the horizontal axis ($h_4 > 0$ and $D_s > 0$). For this region, the transformation for softening response increases continuously only for fractiles beyond either of the two critical points (Equation 18) and decreases continuously between. The transformation for hardening response increases continuously for fractiles between the two critical points (Equation 22) and decreases continuously beyond.

IV. The two coefficients are outside the lower ellipse as well as below the horizontal axis ($h_4 < 0$ and $D_h > 0$). For this region, the transformation for hardening response increases continuously only for fractiles beyond either of the two critical points (Equation 22) and decreases

continuously between. The transformation for softening response increases continuously for fractiles between the two critical points (Equation 18) and decreases continuously beyond.

V. The coefficients lie on the line $h_4 = 0$. The process is non-monotonic and the hermite polynomial reduces to a quadratic. If $h_3 = 0$ then the process is Gaussian.

Three solutions for cases in regions I and II were developed in the original work by Winterstein. A missing inversion for the monotone backward hardening Case (II) is offered here, as are solutions for Cases III and IV (above the practical limit but outside the ovals).

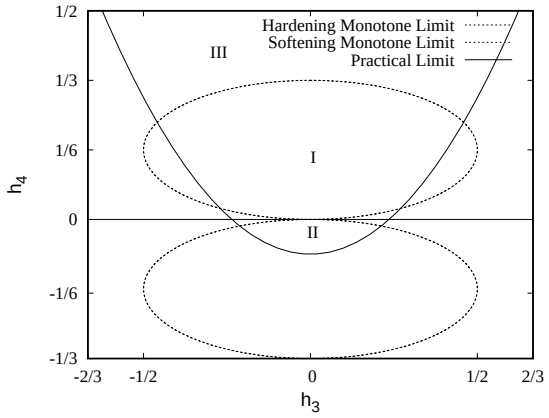

Figure 2: Practical, Softening Monotone and Hardening Monotone Limits in Hermite Moment Space

3.1.1 The Monotone Limit for a Softening Response (Upper Ellipse)

In the model for softening response, the non-Gaussian variable is expressed as a cubic function of the standard Gaussian variable. The slope of Equation 4 is

$$\frac{dx}{du} = \kappa\Big\{3h_4u^2 + 2h_3u + (1 - 3h_4)\Big\} \tag{17}$$

which is a quadratic function. The solutions of the quadratic equation $\frac{dx}{du} = 0$, if any, are the critical points of the cubic function, and play a key role in determining the monotone range. The resulting

critical points are

$$u_c = \frac{-2h_3 \pm \sqrt{4h_3^2 - 12h_4(1-3h_4)}}{6h_4} \tag{18}$$

The existence of these solutions is determined by the discriminant, D_s for the softening case, which is equivalent to the equation inside square root in Equation 18.

$$D_s = 4\Big[h_3^2 - 3h_4(1-3h_4)\Big] \tag{19}$$

A positive discriminant produces two solutions, which implies the curve is non-monotonic, with transitions between the increasing and decreasing parts of the curve at the critical points. Zero discriminant produces one solution (two identical solutions), and a negative discriminant produces no real solution. Since no solution or a single solution to the quadratic equation indicates no critical point in the cubic function, the resulting cubic function with non-positive discriminant is monotone if

$$h_3^2 \leq 3h_4(1-3h_4) \tag{20}$$

The zero discriminant case, $D_s = 0$, can be reorganized to represent the upper ellipse in (h_3, h_4) plane of Figure 2.

$$\frac{h_3^2}{(\frac{1}{2})^2} + \frac{(h_4 - \frac{1}{6})^2}{(\frac{1}{6})^2} = 1 \tag{21}$$

3.1.2 The Monotone Limit for a Hardening Response (Lower Ellipse)

Similarly, the standard Gaussian variable can be expressed as a cubic function of a standardized non-Gaussian variable in the model for hardening response. The same procedure of softening response using Equation 6 results in two critical points, and the discriminant and monotone limit for the hardening case:

$$x_c = \frac{-2h_3 \pm \sqrt{4h_3^2 + 12h_4(1+3h_4)}}{6h_4} \tag{22}$$

$$D_h = 4[h_3^2 + 3h_4(1+3h_4)] \tag{23}$$

$$h_3^2 \leq -3h_4(1+3h_4) \tag{24}$$

Setting $D_h = 0$ in Equation 23 and reorganizing defines the lower ellipse in Figure 2.

$$\frac{h_3^2}{(\frac{1}{2})^2} + \frac{(h_4 + \frac{1}{6})^2}{(\frac{1}{6})^2} = 1 \tag{25}$$

3.2 An Alternative Inversion of the Hermite Polynomial

Here, a new inversion methodology of the original Hermite polynomials (Equations 4 and 6) is offered to enable use of the Hermite model of extreme values in the Cases III and IV, where the polynomial is non-monotone. This new inversion has an important advantage over the original: it enables inversion outside the monotone limit, where multiple solutions are possible. Choosing between these solutions is addressed in Section 3.3. To develop the alternate inversion, the forward transformation for a softening response (Equation 4) is rearranged to a more convenient form:

$$\kappa h_4\Big(u^3 + a_2u^2 + a_1u + a_0\Big) = 0 \tag{26}$$

where $a_0 = \frac{-x-\kappa h_3}{\kappa h_4}$, $a_1 = \frac{1-3h_4}{h_4}$, $a_2 = \frac{h_3}{h_4}$ and x is the value of a non-Gaussian response to be transformed to the Gaussian. The Gaussian equivalent of the specified x is a value of u solving the cubic equation. Among many existing solution approaches, the most practical here is to find its real roots through use of a trigonometric identity [2, 5]. In this solution, the real roots are selected based on computed parameters p and C.

$$p = \frac{3a_1 - a_2^2}{3}; \qquad C = \frac{q}{2}\left(\frac{3}{|p|}\right)^{\frac{3}{2}} \tag{27}$$

where $q = (9a_1a_2 - 27a_0 - 2a_2^3)/27$.

(1) if $p \geq 0$, the equation is monotone and this alternate inversion yields numerical results identical to those of Winterstein (Equation 11), but without restrictions imposed by having a square root of a potentially negative quantity in the solution.

$$u = -\frac{1}{3}a_2 + 2\sqrt{\frac{p}{3}}\sinh\left(\frac{1}{3}\sinh^{-1}C\right) \tag{28}$$

(2) if $p < 0$, the equation is non-monotone and the root selection depends on the value of C.

$$u = -\frac{1}{3}a_2 + 2\sqrt{\frac{|p|}{3}}\cosh\left(\frac{1}{3}\cosh^{-1} C\right) \quad \text{for} \quad C \geq 1 \tag{29}$$

$$u = -\frac{1}{3}a_2 - 2\sqrt{\frac{|p|}{3}}\cosh\left(\frac{1}{3}\cosh^{-1} |C|\right) \quad \text{for} \quad C \leq -1 \tag{30}$$

$$u = -\frac{1}{3}a_2 + 2\sqrt{\frac{|p|}{3}}\cos\left(\frac{1}{3}\cos^{-1} C\right) \quad \text{for} \quad |C| < 1 \tag{31}$$

If the kurtosis of a process is exactly 3, then Equation 4 reduces to a quadratic, and h_4 = 0, which creates a divide by zero in the cubic inversion. The inversion for the quadratic is:

$$u = \frac{-1 \pm \sqrt{1 + 4h_3(h_3 + x/\kappa)}}{2h_3} \tag{32}$$

which increases monotonically if $(\pm)$ is taken as $(+)$ for $h_3 > 0$ and $(-)$ for $h_3 < 0$. This expression can also be used directly with Equation 38 as a three-moment model of extremes.

The inversions for the backward transformation for a hardening response is developed equivalently by rearranging Equation 6.

$$h_4\Big(x^3 + a_2x^2 + a_1x + a_0\Big) = 0 \tag{33}$$

where $a_0 = \frac{-u-h_3}{h_4}$, $a_1 = \frac{1-3h_4}{h_4}$, and $a_2 = \frac{h_3}{h_4}$. Equation 33 is in exactly the same form as Equation 26, so the same solution technique is applied to invert the backward transformation of the hardening response, and the results are nearly identical.

(1) If $p \geq 0$, then the transformation is monotone:

$$x = -\frac{1}{3}a_2 + 2\sqrt{\frac{p}{3}}\sinh\left(\frac{1}{3}\sinh^{-1} C\right) \tag{34}$$

(2) if $p < 0$, the equation is non-monotone and the root selection depends on the value of C.

$$x = -\frac{1}{3}a_2 + 2\sqrt{\frac{|p|}{3}}\cosh\left(\frac{1}{3}\cosh^{-1} C\right) \quad \text{for} \quad C \geq 1 \tag{35}$$

$$x = -\frac{1}{3}a_2 - 2\sqrt{\frac{|p|}{3}}\cosh\left(\frac{1}{3}\cosh^{-1} |C|\right) \quad \text{for} \quad C \leq -1 \tag{36}$$

$$x = -\frac{1}{3}a_2 + 2\sqrt{\frac{|p|}{3}}\cos\left(\frac{1}{3}\cos^{-1} C\right) \quad \text{for} \quad |C| < 1 \tag{37}$$

If the kurtosis is exactly 3, the quadratic inversion is:

$$x = \frac{1 \pm \sqrt{1 + 4h_3(u - h_3)}}{2h_3} \tag{38}$$

which increases monotonically if $(\pm)$ is taken as $(-)$ for $h_3 > 0$ and $(+)$ for $h_3 < 0$.

3.3 Piecewise construction of a Monotone Transformation

In this section, a method is outlined to construct a monotonic transformation by combining the results of non-monotonic hardening and softening transformations over their individual regions of applicability. If two continuous CDF's exist, then there must also exist a final combined transformation that is monotonic at all fractiles, because there must exist a one-to-one mapping between the two distributions such that for any value of u there is exactly one equivalent value of x, and vice versa. The polynomials are non-monotone in regions III and IV, so direct inversion would result in multi-valued transformations at some fractiles. In the cumulative distribution function (CDF), constant fractiles appear as horizontal lines; a transformation between the Gaussian and non-Gaussian at a single fractile appears as a horizontal shift along the constant fractile line. If the transformation is multi-valued, the implication is that there exist multiple crossings of a single fractile of the CDF. The only way multiple crossings can occur is if there is a downward slope in the CDF. By definition, probabilities must be non-negative, so transformations must be monotonic.

The transformation for a monotone case is either hardening or softening over the entire distribution, and either the forward or backward transformation is a cubic polynomial. Non-monotone cases, however, are hardening over some fractiles of the distribution and softening over others. At extreme fractiles (very high or very low), the cubic transformation is dominated by the kurtosis because that term is cubed in Equations 4 and 6; for the transformation to be non-monotone, the skewness term must dominate nearer to the body of the distribution. Such a distribution is either hardening in the kurtosis-controlled extreme tails and softening in the skewness-dominated fractiles nearer to the body of the distribution or vise-versa. Thus, any fractile of a distribution that

can be described by its first four statistical moments can be transformed either to or from a Gaussian using a cubic polynomial because that fractile must be dominated by either the skewness or kurtosis of the process.

A piecewise monotone transformation can be constructed over the entire fractile range by determining the correct fractiles, or points in the x-u transformation space, to transition between the hardening and softening models such that only regions of each model with positive slope are used. Figure 3 shows intersection of non-monotonic cubic polynomials taken from the example presented later in this paper. For forward softening, x is a cubic function of u and for backward hardening, u is a cubic function of x. There are in general as many as nine points of intersection between the two polynomials. Optimal transition points can be readily selected from a plot of the two non-monotone cubic polynomials or these points can be selected numerically. For numerical selection, the forward softening model (Equation 4) and the backward hardening model (Section 3.2) are computed and the critical points for each model (Equations 18 and 22) are identified analytically. These critical points are used to detect a total of three segments on the two curves in which both x and u are increasing, i.e, $\frac{dx}{du}$ and $\frac{du}{dx}$ are both positive.

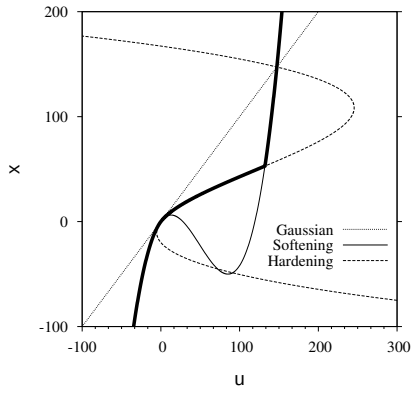

(a) Region III: Softening-Hardening-Softening required for Piecewise Monotone (α_3 = -0.2651, α_4 = 3.0072, t = 4,400 sec)

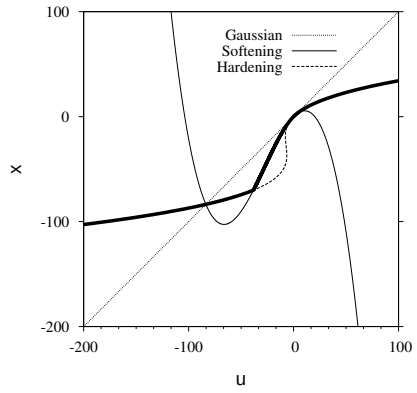

(b) Region IV: Hardening-Softening-Hardening required for Piecewise Monotone (α_3 = -0.2402, α_4 = 2.9885, t = 4,700 sec)

Figure 3: Combination of Non-monotone Hardening and Softening models into a single monotonic transformation

The coefficients of the cubic terms in Equations 4 and 6 are opposite in sign, which guarantees for any $\alpha_4 \neq 3$ that one of the models is increasing at extreme fractiles and the other is decreasing, and non-monotone cubic behavior guarantees opposite slope at more moderate fractiles. There are two overlapping regions of the three increasing segments with an intersection between those segments in each region; these increasing regions must overlap because there must exist a monotonic transformation. Theoretically, the extended model consists of three parts: softening-hardening-softening or hardening-softening-hardening, though quite frequently a two part model is sufficient (softening-hardening or hardening-softening). In practice, a very large but finite range of fractiles must be pre-specified for a numerical search, and in the event a critical point is found to be outside the range, that point is replaced by the end-point of the range. Also, the intersection between the hardening and softening models often creates a discontinuity in the CDF, which would create a jump in the PDF. To avoid this unrealistic behavior, the combined monotonic transformation is smoothed near the intersection. After a piecewise monotonic transformation has been developed, it can be used both forwards and backwards.

In the unlikely event the kurtosis is exactly three, the cubic transformations reduce to quadratics, which are necessarily non-monotone. Monotonic transformations can be easily constructed using the methodology presented here to combine monotonic segments of Equations 32 and 6 or Equations 38 and 4.

4 Application of the Theoretical Developments

The strengths of the original development of the Hermite moment model that helped lead to its widespread use in practical applications is that it is based on a solid theoretical foundation and the resulting equations are extremely simple to implement. The expanded methodology developed in this paper is also reasonably straightforward to implement in a practical application, but not nearly as straightforward as the original, mainly because of the need to identify the points of transition between the hardening and softening models. In cases where existing implementations of the

Hermite model are applicable, this method and the original yield numerically identical results. This new development, however, provides a methodology for cases to which the original is not directly applicable. The numerical scheme described in Section 3.3 has been implemented in Matlab and it is the intent of the authors to make the source code generally available. Two typical applications of the Hermite model are transformations between Gaussian and non-Gaussian equivalents.

4.1 Transformation of a Gaussian fractile to its non-Gaussian Equivalent

In this application, the Hermite moment model is used to predict a pre-specified extreme value of a non-Gaussian process. In such an application, the skewness and kurtosis are calculated directly from the time-history and used to compute the coefficients for the Hermite polynomials (Equations 7). Next, the process is checked against the practical limit (Equation 12). The kurtosis is then checked to determine if the process is hardening or softening, and the monotone limit is checked (Equation 20 or 24). If the process is monotone and hardening, Equation 34 is applicable to calculate the non-Gaussian equivalent to the desired Gaussian fractile; if softening and either monotone or non-monotone, Equation 4 is applicable. If non-monotone hardening, a piecewise monotone transformation must be constructed as outlined in Section 3.3 using Equations 4 and 35–37. Once the transformation has been computed, it can be applied to transform any Gaussian fractile (e.g., the 100-year event) to its non-Gaussian equivalent. The model is valid at every point in the process or distribution, and so can also be used to transform a Gaussian distribution into a general reference shape CDF or PDF conforming to the first four statistical moments of the process.

4.2 Transformation of a non-Gaussian Response to its Gaussian Equivalent

In this application, the Hermite moment model is used to map an equivalent fractile of a process to enable use of traditional statistical tools such as the Student's T-test to compare means of the processes. In such an application, the skewness and kurtosis are again calculated directly from the time-history and used to compute the coefficients for the Hermite polynomials. The process is

checked against the practical limit; the kurtosis is checked to determine if the process is hardening or softening, and the monotone limit is then checked (Equation 20 or 24). If the process is hardening and either monotone or non-monotone, Equation 6 is applicable to calculate the Gaussian equivalent; if monotone and softening, Equation 28 is applicable. If non-monotone softening, a piecewise monotone transformation must be constructed as outlined in Section 3.3 using Equations 6 and 29–31. Once the transformation has been developed, it can be applied to the complete distribution or to every point in the process to transform it to the Gaussian equivalent such that conventional Gaussian statistical tools can be used in place of typically less-powerful non-parametric techniques.

5 EXAMPLE

The Hermite moment model is applied to simulated data resulting from a time-domain solution of a simple numerical model of a Tension Leg Platform (TLP) subject to irregular seas. A TLP is a compliant offshore structure used for production of oil and gas in deep ocean waters that has highly non-Gaussian surge response (horizontal translation in the direction of the environmental loading). The platform is vertically moored by tendons at each of its corners (Figure 4). Surge response time-histories have been simulated using a simplified 2-dimensional nonlinear numerical model, which approximates the Snorre TLP in the Norweigian sector of the North Sea. Environmental conditions were intentionally selected such that the simulated response is very near the intersection of the monotone and non-monotone regions.

5.1 Numerical Model and Simulation of TLP Surge Response

In the numerical model, wave, wind and current forces are applied to a single degree of freedom system including nonlinear restoring force and the equation of motion is solved in the time domain. The two main sources of non-Gaussianity in the model are 1) the non-linear mooring restoring

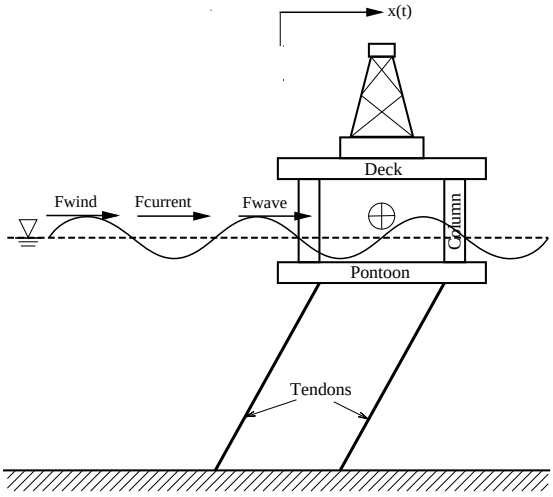

Figure 4: Tension Leg Platform

force caused by the changing angles of the tendons with increased offset and the increased buoyancy of the hull caused by being pulled downward by the tendons, and 2) the non-Gaussian wave forcing caused by the highly nonlinear drag term in the Morison Equation e.g., [16].

5.2 Application of the Hermite Model to Simulation in the Time Domain

Simulations are for a significant wave height of 10.3 m with spectral peak period of 15.5 sec. Wind force and current velocity are held constant at 3×10^7 N and -0.1 m/s, respectively. The time step of integration is 0.05 sec and total time duration for the long time-histories is 90 minutes; in this environment, the natural period is around 72 seconds. Irregularity in the response is due to the random phasing in the wave simulation from a JONSWAP spectrum e.g., [16]. The spectrum was decomposed into a large number of frequency components and wave particle kinematics were computed for each frequency component using Airy theory. Wave kinematics are combined with current velocities at each time-step and hydrodynamic forces are then estimated using the Morison Equation and a constant wind force is added. Finally, the nonlinear equation of motion is solved by time-step integration (Newmark method) [4].

The first four statistical moments of the response ($\mu_Y, \sigma_Y, \alpha_3$ and α_4) have been calculated for

the beginning of the time-history up to specified cut-off times. The first window is from time, t = 0 until t = 200 seconds; the next window is from t = 0 until t = 300 seconds, with each successive window using the entire previous window plus an additional 100 seconds until the final time of 5,400 seconds (90 minutes). The resulting statistical moments are then used with the Hermite model to predict the 1.5-hour mean maximum. In this example, the kurtosis is estimated from the first M points of the time-history using the correction for small samples and not considering statistical dependence between points (e.g., [8]) in which $\alpha_4 \approx [(M+1)\hat{\alpha_4} - 3(M-1)](M-1)/[(M-2)(M-3)] + 3$ where $\hat{\alpha_4} = 1/(M\sigma_X^4)\sum_{m=1}^{M}[X(m) - \mu_X]^4$.

Figure 5 shows prediction results for the 90 minute mean maxima for a single realization of the process as it shifts between solution cases, compared with the equivalent maxima predicted using Gaussian theory only. Table 1 shows the skewness, kurtosis and the behavior of the process. The case presented here was intentionally chosen such that normal variation of the moments within the confidence bands shifts the process between cases. The subsequent smooth behavior of the predicted 1.5-hour maximum shown in Figure 5 is appropriate because each extreme value is the predicted maximum for a single realization of a process; consistent predictions indicate the consistency between four different solution cases of this Hermite model. Prior to this work, there was no Hermite transformation available for cases in the non-monotone regions (Region III or IV in Figure 1). The consistency of results also indicates that for this case, using the previous methodology and taking the closest permissable value of kurtosis would produce results very close to those presented here; applying the prior method with the closest permissable value of kurtosis to cases with larger deviations from the monotone would introduce larger inaccuracies.

Figure 6 shows that the extended model gives consistent results near the kurtosis of 3.0, where the model changes between softening-hardening-softening (S-H-S, 4,400 sec) and hardening-softening-hardening (H-S-H, 4,700 sec,) and softening only (S, 5,000 sec). Results from the three models cannot be differentiated by eye over the entire PDF.

Figure 7 shows a histogram of probability density from a simulation case ending at 4,400 sec-

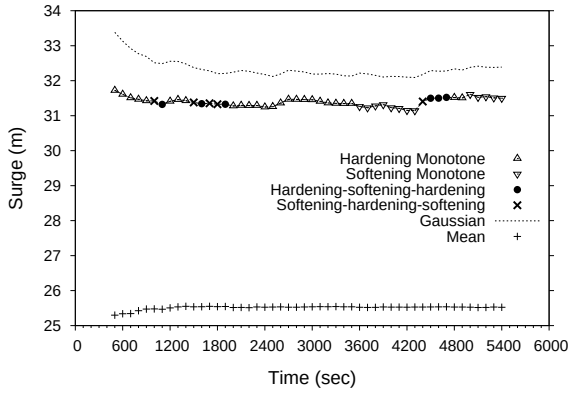

Figure 5: Hermite Extreme Value Estimation: A single realization with statistical moments shifting between monotone and non-monotone models used to predict 90 minute maximum.

Table 1: Resulting Response Moments

Time(sec)	Skewness	Kurtosis	Behavior*
4400	-0.2651	3.0072	S-H-S
4700	-0.2402	2.9885	H-S-H
4900	-0.2417	2.9670	H
5000	-0.2859	3.1169	S

* S = Softening; H = Hardening

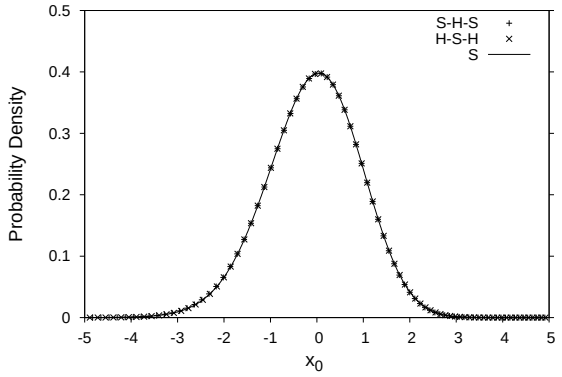

Figure 6: PDF Comparison: standardized softening-hardening-softening, hardening-softening-hardening and monotone responses (4,700 sec, 5,000 sec and 5,300 sec in Table 1)

onds (Table1) compared with two theoretical PDF's. The non-Gaussian PDF is seen to have a much better fit than the Gaussian, especially in the extreme tail, which is generally of highest importance for engineering applications. For this case, the tail appears to be a good fit down to fractiles around 0.001.

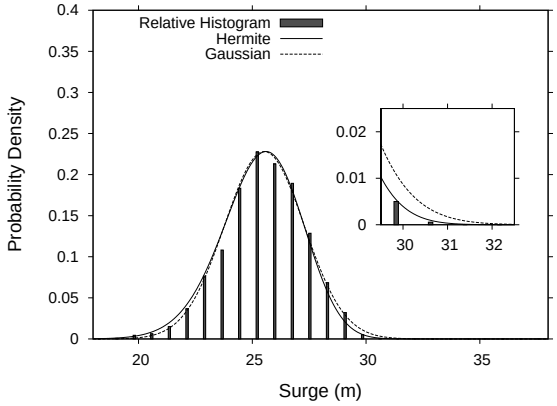

Figure 7: Histogram of 4,100 second simulated response compared with theoretical PDF's based on α_3 = -0.2654, α_4 = 3.0360

Figure 8 compares Hermite model results with extreme value predictions of the 90 minute mean maxima with mean maxima based on Monte Carlo simulation. Each data point is a prediction of the 90 minute mean-maximum based on increasing simulation times, i.e., the point at 1,200 seconds shows a prediction of the 90 minute maximum based on only 20 minutes of measured data. The irregular line with the error bars is the predicted mean-maximum based on the response moments and application of the Hermite model. The error bars indicate $\pm$ one standard deviation and are constructed by computing the statistical moments using data up to the cut-off time for each of the 20 realizations and applying the Hermite model to predict a mean-maximum for each one. The two solid lines are the average of the twenty observed 90-minute maxima $\pm$ one standard deviation. The error bars' being mainly between the horizontal lines indicates reduced variability for maxima predicted using the Hermite model versus maxima computed by direct simulation. The consistent over-prediction of the Gaussian results compared with Hermite and Monte Carlo results (about 0.5 meter) shows that using the Gaussian is overconservative for this negatively skewed case.

Finally, the relatively steady value of the predicted mean maximum indicates that only a relatively small amount of data is needed to compute the statistical moments with sufficient accuracy to predict the expected maximum, and for these cases, only about five minutes of data is necessary for reasonably accurate predictions. The overall conclusion from this figure is that for this case the Hermite model yields more consistent results with comparable accuracy to those produced by direct simulation, and with considerably reduced data and/or computational requirements.

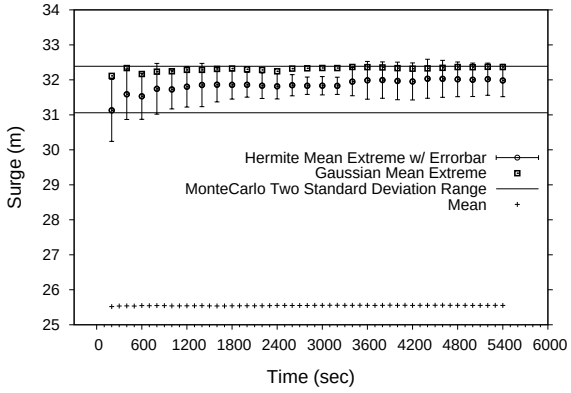

Figure 8: Statistical moments based on short durations used to predict 90 minute maximum. All statistics based on 20 simulations

6 DISCUSSION AND CONCLUSIONS

The Hermite moment model is widely used to transform extreme fractiles between Gaussian and non-Gaussian processes. Historically, the model has been constrained by a monotone limit. Here, the monotone limit is investigated in detail and mathematically expressed as two ellipses in Hermite-coefficient space (Figure 2). An alternate solution technique is offered that overcomes the monotone limitations of the original Hermite moment model, along with one additional monotone case. The work presented here completes the original Hermite moment model for all practical paired values of skewness and kurtosis, and includes mapping between Gaussian and non-Gaussian processes in either direction, subject only to the reasonable limits of second-order theory combined

with first-order Hermite coefficients.

The major innovation offered in this paper is a new methodology by which the Hermite model can be applied to highly skewed cases with near-Gaussian kurtosis, which are associated with non-monotone cubic polynomial transformations (Section 3.3). In non-monotone regions, the new methodology combines monotonic segments of a cubic polynomial with monotonic segments of the inversion of another cubic polynomial to create one complete monotonic transformation over the entire fractile range. For the forward model, the increasing parts of the cubic polynomial (Equation 4) are combined with the increasing parts of the inversion (Equations 35–37). For the backward model, the increasing parts of Equation 6 are combined with the increasing parts of Equations 29–31.

Additionally, a new inversion of the backward model is developed as a solution for the forward hardening monotone case (Equation 34). This inversion was excluded from the original work by Winterstein [19, 20]. For consistency, an equivalent inversion is also proposed for monotone softening, which yields the same result as the original formulation.

The new technique is demonstrated through application to simulated irregular motions of a tension leg platform (TLP). The simulated process is non-Gaussian and the environmental conditions were selected such that variability of sample response moments caused the response to shift between regions in which the monotone, softening-hardening-softening and hardening-softening-hardening solutions apply. Results show that the model transitions smoothly between these regions. Predictions of extreme responses are shown to be more accurate than application of a Gaussian model alone, and require less data and show less variability than averaging the observed maxima of twenty simulations.

ACKNOWLEDGMENTS

This work was supported by the National Science Foundation, Division of Civil and Mechanical Systems under Agreement Numbers CMS-0428585 and CMS-0448730. Any opinions, findings,

and conclusions or recommendations expressed in this material are those of the authors and do not necessarily reflect the view of the National Science Foundation.

References

[1] Atalik, T. S. and Utku, S. (1976). Stochastic linearization of multi-degree-of-freedom nonlinear systems. *Earthquake Engineering & Structural Dynamics*, 4(4):411–420.

[2] Birkhoff, G. and Mac Lane, S. (1996). *A Survey of Modern Algebra*. Macmillan, New York, 5 th edition.

[3] Caughey, T. K. (1963). Equivalent linearization techniques. *Journal of the Acoustical Society of America*, 35(11):1706–1711.

[4] Chopra, A. K. (2001). *Dynamics of Structures: Theory and Applications to Earthquake Engineering*. Prentice Hall.

[5] Dickson, L. E. (1914). *Elementary Theory of Equations*. Wiley, New York.

[6] Grigoriu, M. (1984). Crossings of non-gaussian translation processes. *Journal of Engineering Mechanics*, 110(4):610–620.

[7] Jensen, J. J. (1994). Dynamic amplification of offshore steel platform responses due to non-gaussian wave loads. *Marine Structures*, 7:91–105.

[8] Joanes, D. N. and Gill, C. A. (1988). Comparing measures of sample skewness and kurtosis. *Journal of Royal Statistical Society*, 47:183–189.

[9] Lange, C. H. (1996). *Probabilistic Fatigue Methodology and Wind Turbine Reliability*. PhD thesis, Stanford University.

[10] Mansour, A. E. and Jensen, J. J. (1995). Slightly non-linear extreme loads and load combinations. *Journal of Ship Research*, 39(2):139–149.

[11] Moarefzadeha, M. and Melchers, R. (2006). Nonlinear wave theory in reliability analysis of offshore structures. *Probabilistic Engineering Mechanics*, 21(2):99–111.

[12] Murotsu, Y., Okada, H., Kishi, M., Yonezawa, M., and Niwa, K. (1981). Fourth order moment approximation to reliability of non-linear structure. In *Transaction of the Sixth International Conference on Structural Mechanics in Reactor Technology*, Paris, France. Paper No. M12.

[13] Ochi, M. (1986). Non-gaussian random processes in ocean engineering. *Probabilistic Engineering Mechanics*, 1(1):28–39.

[14] Peeringa, J. (2003). Extrapolation of extreme responses of a multi megawatt wind turbine. Technical report, Energy Research Centre of the Netherlands. ECN-C–03-131.

[15] Puig, B. and Akian, J. (2004). Non-gaussian simulation using hermite polynomials expansion and maximum entropy principle. *Probabilistic Engineering Mechanics*, 19:293–305.

[16] Sarpkaya, T. and Issacson, M. (1981). *Mechanics of Wave Forces on Offshore Structures*. Van Nostrand Reinhold.

[17] Soize, C. (1978). Gust loading factors with nonlinear pressure terms. *Journal of the Structural Division, ASCE*, 104:991–1007. No. ST6.

[18] Spanos, P. (1981). Stochastic linearization in structural dynamics. *Applied Mechanics Review*, 34(1):1–8.

[19] Winterstein, S. R. (1987). Moment-based hermite models of random vibration. Report 219, Department of Structural Engineering, Technical University of Denmark.

[20] Winterstein, S. R. (1988). Nonlinear vibration models for extremes and fatigue. *Journal of Engineering Mechanics*, 114(10):1772–1790. ISSN 0733-3-9399/88/0010-1772, Paper No. 22855.

[21] Winterstein, S. R. and Lange, C. H. (1995). Moment-based probability models for wind engineering applications. In *Proceedings of 10th Engineering Mechanics Speciality Conference, ASCE*, volume 1, pages 159–162.

[22] Winterstein, S. R., Ude, T. C., and Kleiven, G. (1994). Springing and slow-drift responses: Predicted extremes and fatigue vs. simulation. In *Behaviour of Off-Shore Structures 1994: Proceedings of the international conference: BOSS 94*, volume 3, pages 1–15, MIT, Cambridge, USA.

Captions

Figure 1: Various Regions of Model Applicability

Figure 2: Practical, Softening Monotone and Hardening Monotone Limits in Hermite Moment Space

Figure 3: Combination of Non-monotone Hardening and Softening models into a single monotonic transformation

(a) Region III: Softening-Hardening-Softening required for Piecewise Monotone (α_3 = -0.2651, α_4 = 3.0072, t = 4,400 sec)

(b) Region IV: Hardening-Softening-Hardening required for Piecewise Monotone (α_3 = -0.2402, α_4 = 2.9885, t = 4,700 sec)

Figure 4: Tension Leg Platform

Figure 5: Hermite Extreme Value Estimation: A single realization with statistical moments shifting between monotone and non-monotone models used to predict 90 minute maximum.

Figure 6: PDF Comparison: standardized softening-hardening-softening, hardening-softeninghardening and monotone responses (4,700 sec, 5,000 sec and 5,300 sec in Table 1)

Figure 7: Histogram of 4,100 second simulated response compared with theoretical PDFs based on α_3 = -0.2654, α_4 = 3.0360

Figure 8: Statistical moments based on short durations used to predict 90 minute maximum. All statistics based on 20 simulations

Table 1: Resulting Response Moments